Morphology–Transport Relations for Packed Beds: From Metric Properties to Structural Descriptors of Diffusion and Hydrodynamic Dispersion

Philipps Universität Marburg

Siarhei Khirevich, Stefan Bruns, Alexandra Höltzel, and Ulrich Tallarek

Department of Chemistry, Philipps-Universität Marburg, Hans-Meerwein-Strasse, 35032 Marburg, Germany
e-mail: khirevich@gmail.com, tallarek@staff.uni-marburg.de

Introduction

Over last decades computer simulations became a powerful tool for understanding and quantification transport in various porous media including chromatography columns. In our work we perform three-dimensional simulations of flow, diffusion, and hydrodynamic dispersion in computer generated and physically reconstructed [1] packings of closely-packed spherical particles. The former proved to be a good model for systematic investigation of transport in particulate columns, while the latter actually contains information on the real-life pore structure of packed microcapillary and acts as a validation geometry for computer simulations. For three-dimensional reconstruction we employed confocal laser scanning microscopy (CLSM) which enabled assessment of the capillary pore space with high resolution (30nm per voxel or 66 voxels per average particle diameter), and, after successive analysis of the scanned images, obtaining coordinates and diameters of particles in capillary, as well as centers and semi axes of ellipses approximating the capillary wall. This geometrical information was enough to perform practically resolution-independent simulations of transport using powerful numerical tools (lattice Boltzmann and random walk particle tracking methods) and state-of-the-art supercomputing facilities. In this work we compare simulated transport coefficients (permeability and hydrodynamic dispersion/plate height) with the available experimental data, and perform detailed analysis of the pore-space geometry and velocity flow fields.

Simulation geometry

First packing considered in this study is the physical reconstruction of $10\,\mu$m i.d. capillary packed with $2\,\mu$m particles. On the initial step, one stack of 450 images (individual image cut is shown below)

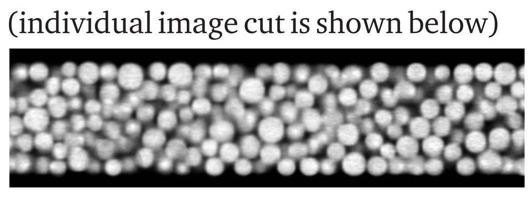

was acquired using CLSM; the stack length was 8192 pixels (246 µm). Thereafter four such image stacks were collected and combined together using their overlapping regions in order to obtain one long 3D image of a capillary segment with the length of ~28000 pixels (840 µm).

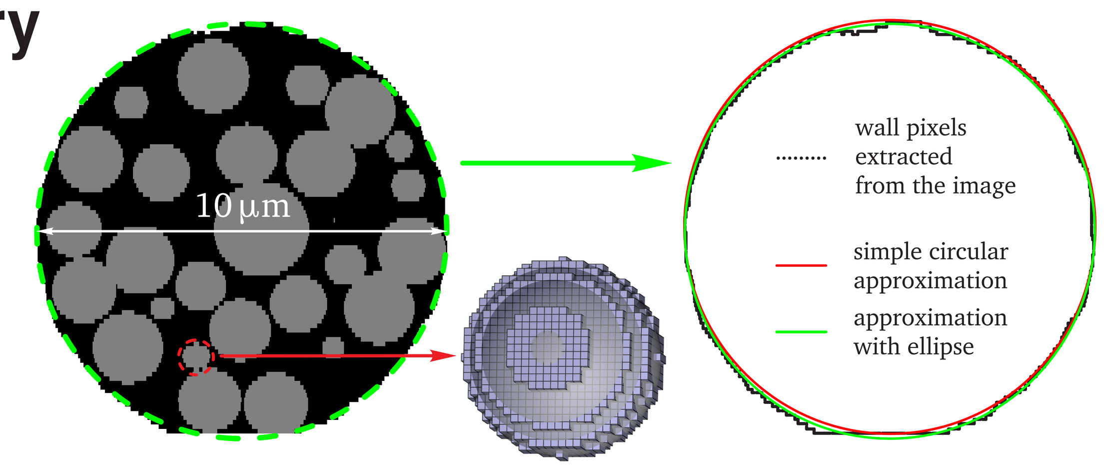

Figure 1. Left: cross section of a reconstructed image stack after processing. Middle: example of a small sphere fit to the closely located set of pixels extracted from the images. Right: wall pixels extracted from the image on the left with the corresponding approximations using circle and ellipse.

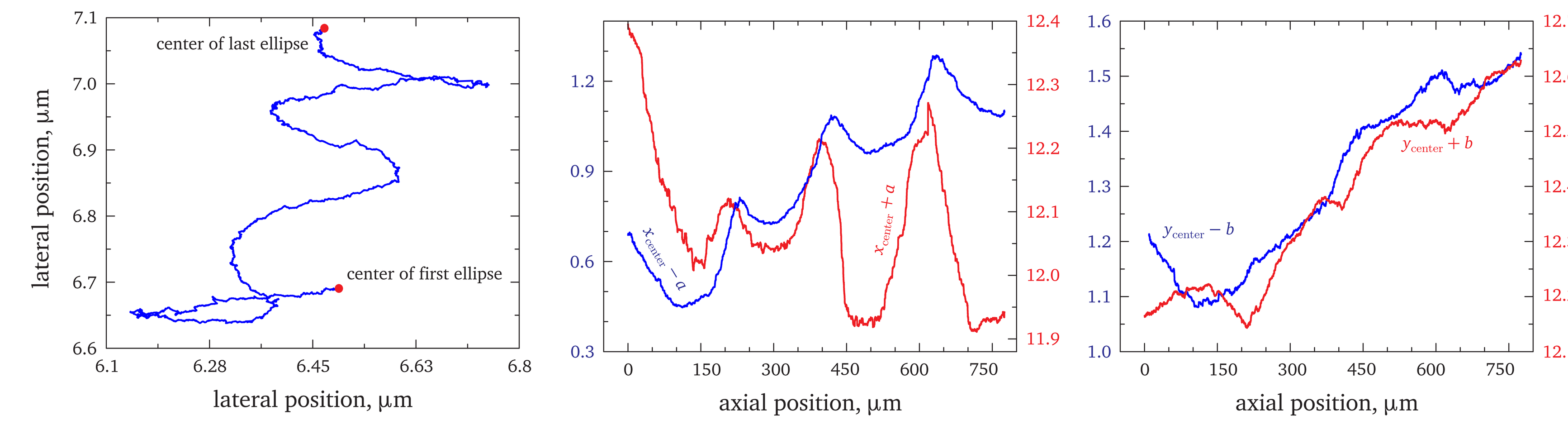

Figure 2. Wall in each cross-sectional image of a real-life capillary was approximated using ellipse with four parameters, two for its center (x_{center}, y_{center}) and two for the semi axes (a, b). The reconstructed capillary exposed axial and lateral deviations from the perfect cylindrical geometry, and this figure provides quantification of these deviations based on the parameters of the fitted ellipses. Left: lateral deviation of x_{center} and y_{center} over the whole length of the reconstructed domain. Middle (Right): leftmost and rightmost (bottommost and topmost) points of the ellipses collected over the whole reconstructed domain. In the following geometrical analysis the spatial inhomogeneity of the confining wall was taken into consideration.

Figure 3. Side view on the reconstructed packing used in simulations. The packing contains 9601 particles, has the length of 390 particles diameters, and its average porosity is 0.448.

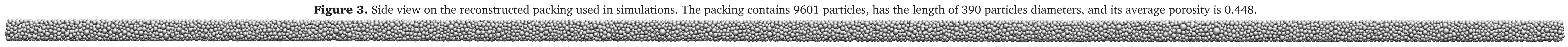

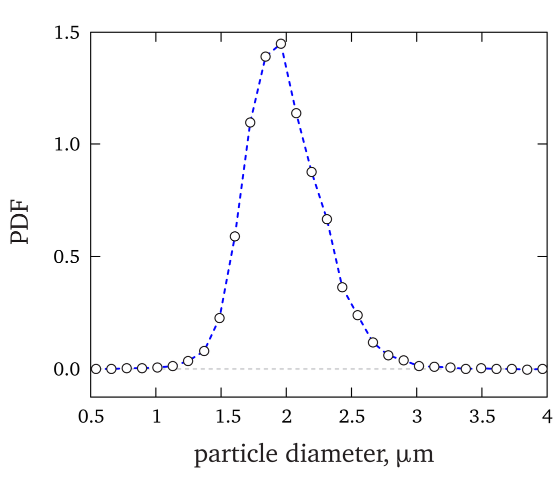

Figure 4. Probability density (distribution) function of the reconstructed particle diameters. The data were collected using a sample of 9601 particle diameters. All the packings considered in this study use the same fixed set of particles diameters. Relative standard deviation of the distribution is 15.7%.

The second set of packings was generated in order to complement the original reconstructed packing. Using Jodrey–Tory algorithm, we generated two packings with different degree of heterogeneity (heterogeneous Rx0.001 and homogeneous Sx2). Both packings used the reconstructed set of particle diameters (d_p), and were confined by circular (i.e., non-elliptical) wall. Inner diameter of the confining cylinder (=5.65 d_p) was chosen to match the average porosity value of the reconstructed packing (=0.448).

As demonstrated in Figure 1, approximation of the scanned geometry with spheres and ellipses slightly differs from the geometry of the original scanned images. To address the possible influence of the approximation with spheres and ellipses, we performed additional simulations using only the original bitmap images (one of which is shown on the left part of Figure 1). The simulations performed in this geometry are referred to as “scanned”, while “reconst.” denotes the packing formed by spheres and ellipses.

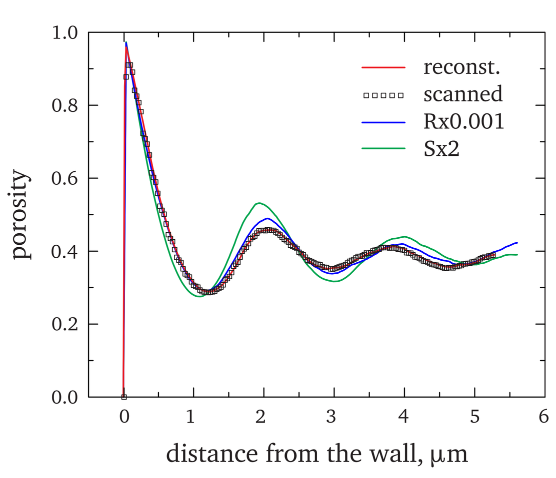

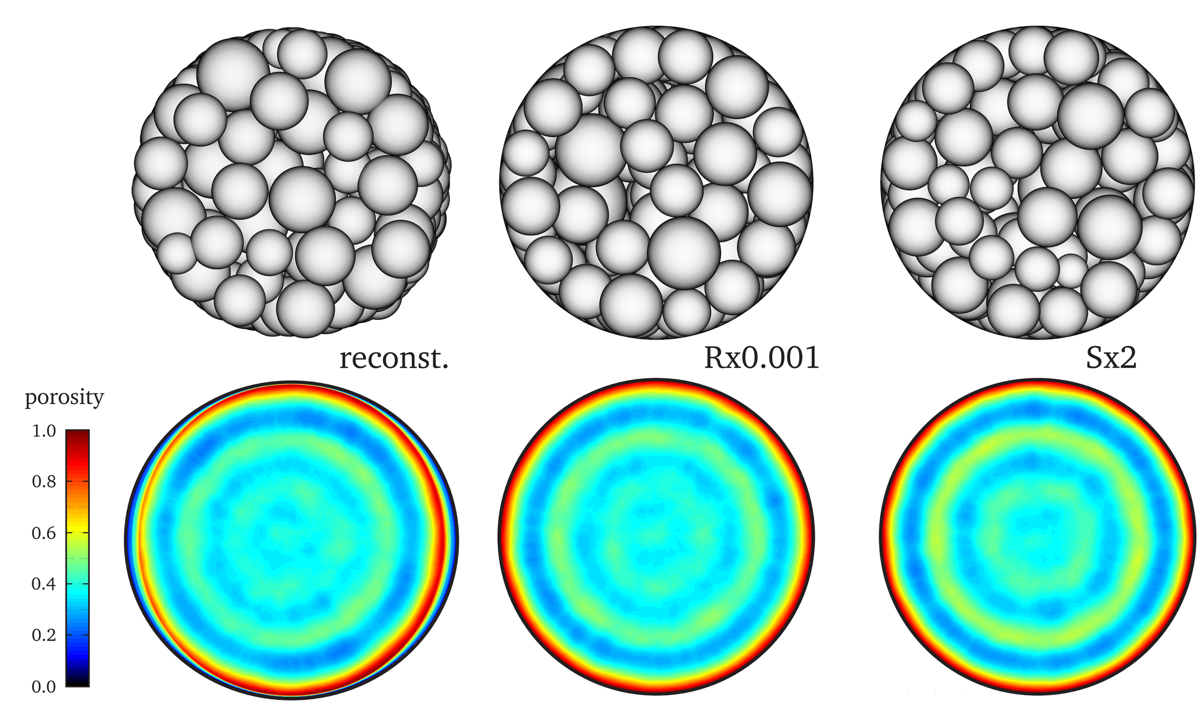

Figure 5. Top-left: average porosity profiles for the reconstructed (reconst. and scanned) and generated (Rx0.001 and Sx2) packings. Right: front view (top) onto the packing, and the corresponding two-dimensional porosity profiles (bottom).

Simulation of flow and diffusion

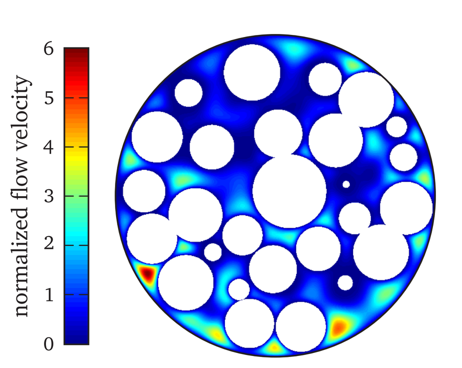

Figure 6. Axial flow velocity profile for the packing region close to the one shown in Figure 1. The presented local velocities are normalized by their global average value.

Reconstructed and generated packings were descretized with high spatial resolution of 100 pixels/d_p, resulting in the lattice dimensions of about 600 x 600 x 40000 pixels. The lattice Boltzmann method was used to simulate slow flow of an incompressible fluid in the voids of the packings. Diffusion simulations were done using the random walk particle tracking method. Determined values of permeability and effective diffusion coefficient are presented in the table on the right. Figure 7b provides comparison of the simulated permeabilities with experimental data.

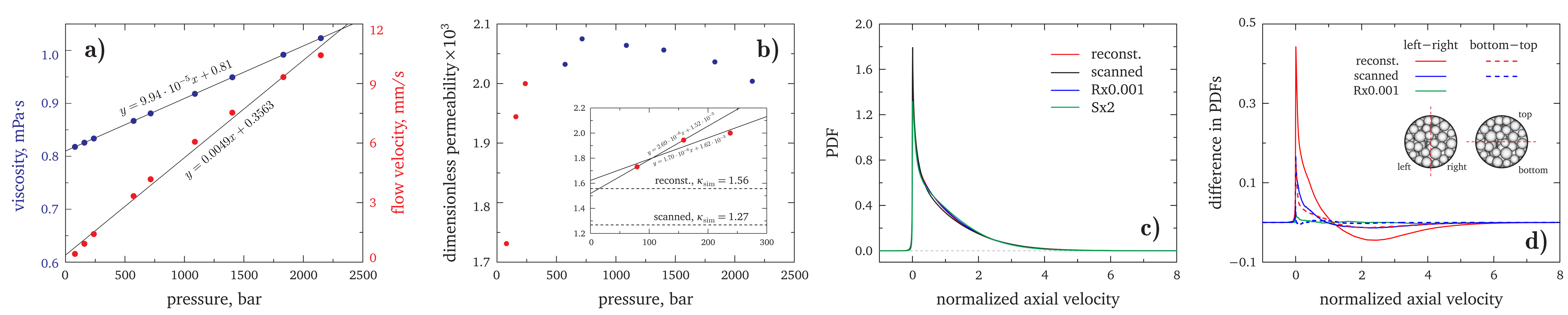

Figure 7. a) Experimentally determined values of the mobile phase viscosity and velocity (data provided by J. Grinias, J. Jorgenson’s group). Due to high values of the applied pressure, with increase of pressure viscosity demonstrates linear growth while mobile phase velocity — non-linear [2]. **b)** Dimensionless permeability calculated using the experimentally determined viscosity and flow velocity, and value of the applied pressure. The inset shows the first three permeability points with the corresponding linear fits. **c,d)** Velocity distribution functions for the indicated packings.

	dimensionless permeability	effective diffusion coefficient
reconst.	1.56×10^{-3}	0.72
scanned	1.27×10^{-3}	0.69
Rx0.001	1.39×10^{-3}	0.72
Sx2	1.39×10^{-3}	0.72

Simulation of hydrodynamic dispersion

After flow simulation is completed, calculated stationary three-dimensional flow field is stored a into file, and these data, together with the simulation geometry, are used as input for the dispersion simulations.

Simulation of hydrodynamic dispersion was performed similarly to the diffusion simulations, using the random walk particle tracking method (RWPT). The method distributes a large amount of small tracers in the void space of a packing, and on each iteration displaces each tracer a small distance due to advection (calculated using the know velocity field) and diffusion (normally distributed random numbers). Hydrodynamic dispersion coefficient (and the corresponding plate height value) is determined based on the statistical moments of the tracer ensemble. Our simulations assume particles have hard wall (i.e., a tracer cannot enter the particle).

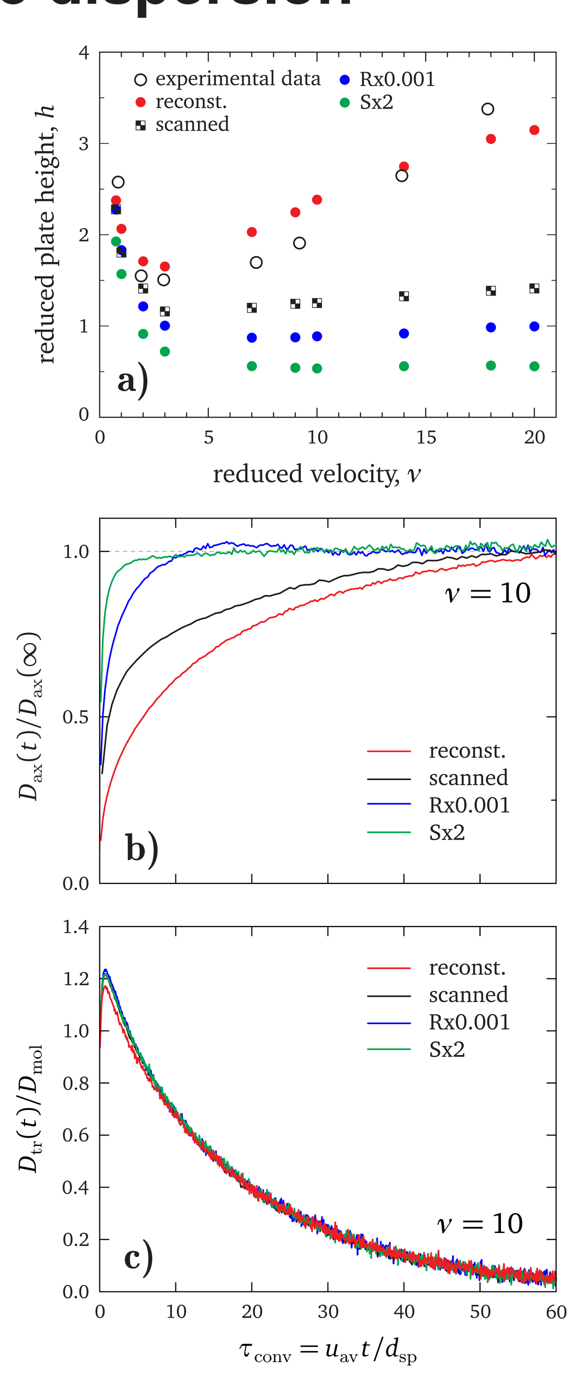

Figure 8. a) Comparison of the reduced plate height values in the generated and reconstructed packings with the experimental data (the latter are provided by J. Grinias, J. Jorgenson’s group [3]). **b,c)** Time evolution of the *normalized* longitudinal (D_{ax}) and transverse (D_{tr}) dispersion coefficients as a function of the dimensionless convective time (one unit corresponds to the time needed for non-retained tracer moving with the average flow velocity to travel the distance of one (average) particle diameter). Data are shown for the fixed flow rate. In the cylindrical column with axial symmetry cylinder radius (diameter) determines the time needed for D_{ax} (D_{tr}) to reach its asymptotic value (non-zero for D_{ax} and zero for D_{tr}) [4], and therefore axial dispersion reaches its plateau four times faster than transverse one. This is actually seen for generated Rx0.001 and Sx2 packings. On the other hand, both reconstructed packings demonstrate approximately *identical* asymptotic times for D_{ax} and D_{tr}, resulting from asymmetrical distribution of voids relative to the axis (see Figures 5 and 9).

Voronoi tessellation

Voronoi tessellation is a powerful approach for analysis of the void space of particulate packings, and it is an alternative to the common analysis based on porosity profiles. The idea behind Voronoi tessellation is to determine a set of space points closer to the *center* of a given sphere than to any of its neighbours. Recently, we demonstrated a great potential of Voronoi tessellation in correlating pore-space geometry with dispersion for the packings of equal particles [5]. In the case of unequal particle diameters (see Figure 4) original Voronoi tessellation can be extended to the S-Voronoi tessellation where space points closer to the *surface* of a given sphere are now considered. In this study we apply S-Voronoi tessellation to the reconstructed and generated packings, and the results of the geometrical analysis are presented in Figure 9.

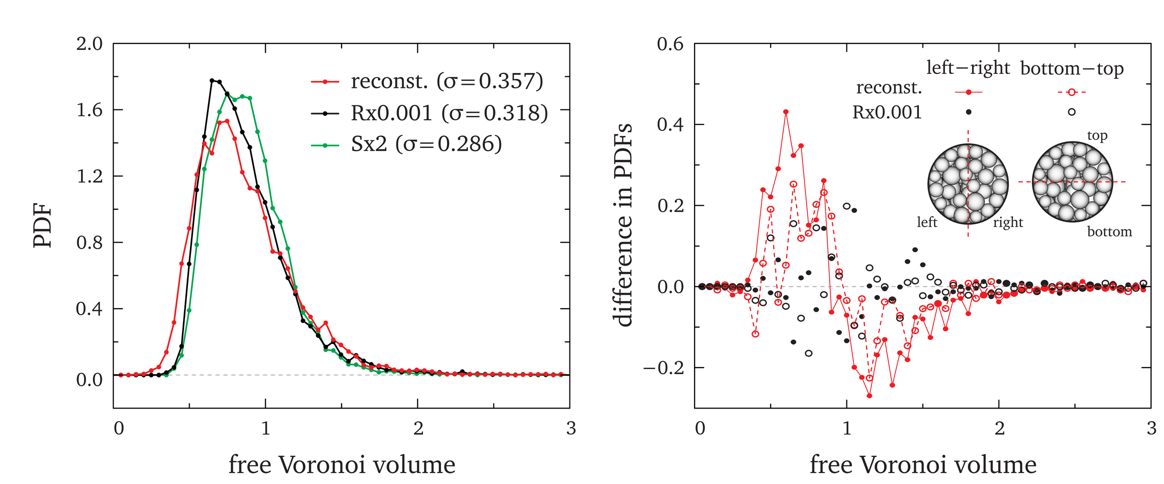

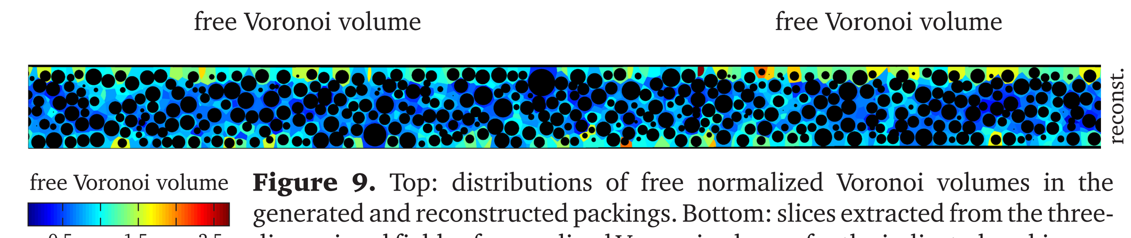

Figure 9. Top: distributions of free normalized Voronoi volumes in the generated and reconstructed packings. Bottom: slices extracted from the three-dimensional fields of normalized Voronoi volumes for the indicated packings.

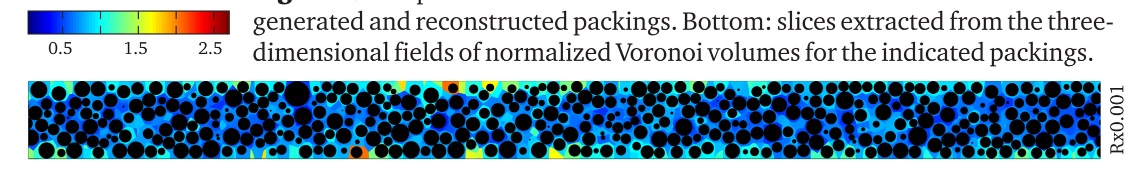

Conclusion

We performed high-resolution simulations of flow, diffusion, and hydrodynamic dispersion in two reconstructed and two generated geometries. One reconstructed geometry was based on the direct imaging of the pore space of particulate capillary, while another resulted from an additional post-processing of the images (giving locations and diameters of particles as well as approximation of the capillary wall with a large set of ellipses). Two additional computer-generated packings were created with the basic geometrical properties (average porosity, inner diameter of the confining cylindrical container, particle size distribution) taken from the reconstructed packing.

Comparison of the permeability values revealed excellent agreement between experiment and simulation in the second reconstructed packing. Dispersion simulations resulted in surprisingly high difference between two reconstructed packings as well as between the second reconstructed and computer-generated ones. The observed difference can be explained by the reduced axial symmetry in two reconstructed packings (which is supported by Figures 7d, 8b, 9), and better resolved near-wall region of the second packing (Figure 5) amplifies this effect further. Much lower plate height values (Figure 8a) of the simulated packings demonstrate high potential of particulate packings on a way to increase the separation efficiency.

Acknowledgments

Computational resources on IBM BlueGene/Q platform were provided by “Juqueen” installed at FZJ (Forschungszentrum Jülich, Germany). We are grateful to the Jülich Supercomputing Centre (JSC) for allocation of a special CPU-time grant (project HMR10). We thank James Grinias for providing experimental permeability and plate height data.

References

[1] Bruns, S.; Tallarek, U. *J. Chromatogr. A*, **1218**: 1849–1860. 2011.
[2] Kaiser, T. J. et al. *Anal. Chem.*, **81**: 2860–2868, 2009.
[3] Bruns, S. et al. *Anal. Chem.*, **84**: 4496–4503, 2012.
[4] Khirevich, S. et al. *Anal. Chem.*, **81**: 7057–7066, 2009.
[5] Khirevich, S. et al. *J. Chromatogr. A*, **1217**: 4713–4722. 2010.